Available online at www.sciencedirect.com
ScienceDirect
Astroparticle Physics 29 (2008) 243–256
Astroparticle Physics
www.elsevier.com/locate/astropart

Upper limit on the cosmic-ray photon flux above 10^{19} eV using the surface detector of the Pierre Auger Observatory

Pierre Auger Collaboration

J. Abraham [n], P. Abreu [bm], M. Aglietta [ay], C. Aguirre [q], D. Allard [af], I. Allekotte [g], J. Allen [cf], P. Allison [ch], J. Alvarez-Muñiz [bt], M. Ambrosio [bb], L. Anchordoqui [cu,cg], S. Andringa [bm], A. Anzalone [ax], C. Aramo [bb], S. Argirò [aw], K. Arisaka [ck], E. Armengaud [af], F. Arneodo [az], F. Arqueros [bq], T. Asch [al], H. Asorey [e], P. Assis [bm], B.S. Atulugama [ci], J. Aublin [ah], M. Ave [cl], G. Avila [m], T. Bäcker [ap], D. Badagnani [j], A.F. Barbosa [s], D. Barnhill [ck], S.L.C. Barroso [x], P. Bauleo [ca], J.J. Beatty [ch], T. Beau [af], B.R. Becker [cq], K.H. Becker [aj], J.A. Bellido [ci], S. BenZvi [ct], C. Berat [ai], T. Bergmann [ao], P. Bernardini [as], X. Bertou [e], P.L. Biermann [am], P. Billoir [ah], O. Blanch-Bigas [ah], F. Blanco [bq], P. Blasi [cc,aq,ba], C. Bleve [bw], H. Blümer [ao,ak], M. Boháčová [ad], C. Bonifazi [ah,s], R. Bonino [ay], M. Boratav [ah], J. Brack [ca,cm], P. Brogueira [bm], W.C. Brown [cb], P. Buchholz [ap], A. Bueno [bs], R.E. Burton [by], N.G. Busca [af], K.S. Caballero-Mora [ao], B. Cai [co], D.V. Camin [ar], L. Caramete [am], R. Caruso [av], W. Carvalho [u], A. Castellina [ay], O. Catalano [ax], G. Cataldi [as], L. Cazon [cl], R. Cester [aw], J. Chauvin [ai], A. Chiavassa [ay], J.A. Chinellato [v], A. Chou [cf,cc], J. Chye [ce], P.D.J. Clark [bv], R.W. Clay [p], E. Colombo [b], R. Conceição [bm], B. Connolly [cr], F. Contreras [l], J. Coppens [bg,bi], A. Cordier [ag], U. Cotti [be], S. Coutu [ci], C.E. Covault [by], A. Creusot [bo], A. Criss [ci], J. Cronin [cl], A. Curutiu [am], S. Dagoret-Campagne [ag], K. Daumiller [ak], B.R. Dawson [p], R.M. de Almeida [v], C. De Donato [ar], S.J. de Jong [bg], G. De La Vega [o], W.J.M. de Mello Junior [v], J.R.T. de Mello Neto [cl,aa], I. De Mitri [as], V. de Souza [ao], L. del Peral [br], O. Deligny [ae], A. Della Selva [at], C. Delle Fratte [au], H. Dembinski [an], C. Di Giulio [au], J.C. Diaz [ce], C. Dobrigkeit [v], J.C. D'Olivo [bf], D. Dornic [ae], A. Dorofeev [cd], J.C. dos Anjos [s], M.T. Dova [j], D. D'Urso [at], I. Dutan [am], M.A. DuVernois [cn], R. Engel [ak], L. Epele [j], M. Erdmann [an], C.O. Escobar [v], A. Etchegoyen [c], P. Facal San Luis [bt], H. Falcke [bg,bj], G. Farrar [cf], A.C. Fauth [v], N. Fazzini [cc], F. Ferrer [by], S. Ferry [bo], B. Fick [ce], A. Filevich [b], A. Filipčič [bn], I. Fleck [ap], R. Fonte [av], C.E. Fracchiolla [t], W. Fulgione [ay], B. García [n], D. García Gámez [bs], D. Garcia-Pinto [bq], X. Garrido [ag], H. Geenen [aj], G. Gelmini [ck], H. Gemmeke [al], P.L. Ghia [ae,ay], M. Giller [bl], H. Glass [cc], M.S. Gold [cq], G. Golup [f], F. Gomez Albarracin [j], M. Gómez Berisso [f], R. Gómez Herrero [br], P. Gonçalves [bm], M. Gonçalves do Amaral [ab], D. Gonzalez [ao], J.G. Gonzalez [cd], M. González [bd], D. Góra [ao,bk], A. Gorgi [ay], P. Gouffon [u], V. Grassi [ar], A.F. Grillo [az], C. Grunfeld [j], Y. Guardincerri [h], F. Guarino [at], G.P. Guedes [w], J. Gutiérrez [br], J.D. Hague [cq], J.C. Hamilton [af], P. Hansen [bt], D. Harari [f], S. Harmsma [bh], J.L. Harton [ae,ca], A. Haungs [ak], T. Hauschildt [ay], M.D. Healy [ck], T. Hebbeker [an], G. Hebrero [br], D. Heck [ak], , C. Hojvat [cc], V.C. Holmes [p], P. Homola [bk], J. Hörandel [bg], A. Horneffer [bg], M. Horvat [bo], M. Hrabovský [ad], T. Huege [ak], M. Hussain [bo], M. Iarlori [aq], A. Insolia [av], F. Ionita [cl],

0927-6505/$ - see front matter
doi:10.1016/j.astropartphys.2008.01.003

A. Italiano [av], M. Kaducak [cc], K.H. Kampert [aj], T. Karova [ad], B. Kégl [ag], B. Keilhauer [ao], E. Kemp [v], R.M. Kieckhafer [ce], H.O. Klages [ak], M. Kleifges [al], J. Kleinfeller [ak], R. Knapik [ca], J. Knapp [bw], D.-H. Koang [ai], A. Krieger [b], O. Krömer [al], D. Kuempel [aj], N. Kunka [al], A. Kusenko [ck], G. La Rosa [ax], C. Lachaud [af], B.L. Lago [aa], D. Lebrun [ai], P. Lebrun [cc], J. Lee [ck], M.A. Leigui de Oliveira [z], A. Letessier-Selvon [ah], M. Leuthold [an], I. Lhenry-Yvon [ae], R. López [bc], A. Lopez Agüera [bt], J. Lozano Bahilo [bs], R. Luna García [bd], M.C. Maccarone [ax], C. Macolino [aq], S. Maldera [ay], G. Mancarella [as], M.E. Manceñido [j], D. Mandat [ad], P. Mantsch [cc], A.G. Mariazzi [j], I.C. Maris [ao], H.R. Marquez Falcon [be], D. Martello [as], J. Martínez [bd], O. Martínez Bravo [bc], H.J. Mathes [ak], J. Matthews [cd,cj], J.A.J. Matthews [cq], G. Matthiae [au], D. Maurizio [aw], P.O. Mazur [cc], T. McCauley [cg], M. McEwen [br,cd], R.R. McNeil [cd], M.C. Medina [c], G. Medina-Tanco [bf], A. Meli [am], D. Melo [b], E. Menichetti [aw], A. Menschikov [al], Chr. Meurer [ak], R. Meyhandan [bh], M.I. Micheletti [c], G. Miele [at], W. Miller [cq], S. Mollerach [f], M. Monasor [bq,br], D. Monnier Ragaigne [ag], F. Montanet [ai], B. Morales [bf], C. Morello [ay], J.C. Moreno [j], C. Morris [ch], M. Mostafá [cs], M.A. Muller [v], R. Mussa [aw], G. Navarra [ay], J.L. Navarro [bs], S. Navas [bs], P. Necesal [ad], L. Nellen [bf], C. Newman-Holmes [cc], D. Newton [bw,bt], N.T. Thao [cv], N. Nierstenhoefer [aj], D. Nitz [ce], D. Nosek [ac], L. Nožka [ad], J. Oehlschläger [ak], T. Ohnuki [ck], A. Olinto [af,cl], V.M. Olmos-Gilbaja [bt], M. Ortiz [bq], F. Ortolani [au], S. Ostapchenko [ao], L. Otero [n], N. Pacheco [br], D. Pakk Selmi-Dei [v], M. Palatka [ad], J. Pallotta [a], G. Parente [bt], E. Parizot [af], S. Parlati [az], S. Pastor [bp], M. Patel [bw], T. Paul [cg], V. Pavlidou [cl], K. Payet [ai], M. Pech [ad], J. Pękala [bk], R. Pelayo [bd], I.M. Pepe [y], L. Perrone [as], S. Petrera [aq], P. Petrinca [au], Y. Petrov [ca], P.N. Diep [cv], P.N. Dong [cv], P.T. Nhung [cv], A. Pichel [k], R. Piegaia [h], T. Pierog [ak], M. Pimenta [bm], T. Pinto [bp], V. Pirronello [av], O. Pisanti [at], M. Platino [b], J. Pochon [e], P. Privitera [au], M. Prouza [ad], E.J. Quel [a], J. Rautenberg [aj], A. Redondo [br], S. Reucroft [cg], B. Revenu [af], F.A.S. Rezende [s], J. Ridky [ad], S. Riggi [av], M. Risse [aj], C. Rivière [ai], V. Rizi [aq], M. Roberts [ci], C. Robledo [bc], G. Rodriguez [bt], M.D. Rodríguez-Frías [br], J. Rodriguez Martino [av], J. Rodriguez Rojo [l], I. Rodriguez-Cabo [bt], G. Ros [bq,br], J. Rosado [bq], M. Roth [ak], C. Roucelle [ah], B. Rouillé-d'Orfeuil [af], E. Roulet [f], A.C. Rovero [k], F. Salamida [aq], H. Salazar [bc], G. Salina [au], F. Sánchez [bf], M. Santander [l], C.E. Santo [bm], E.M. Santos [ah,s], F. Sarazin [bz], S. Sarkar [bu], R. Sato [l], V. Scherini [aj], H. Schieler [ak], A. Schmidt [al], F. Schmidt [cl], T. Schmidt [ao], O. Scholten [bh], P. Schovánek [ad], F. Schüssler [ak], S.J. Sciutto [j], M. Scuderi [av], A. Segreto [ax], D. Semikoz [af], M. Settimo [as], R.C. Shellard [s,t], I. Sidelnik [c], B.B. Siffert [aa], G. Sigl [af], N. Smetniansky De Grande [b], A. Smiałkowski [bl], R. Šmída [ad], A.G.K. Smith [p], B.E. Smith [bw], G.R. Snow [cp], P. Sokolsky [cs], P. Sommers [ci], J. Sorokin [p], H. Spinka [bx,cc], R. Squartini [l], E. Strazzeri [au], A. Stutz [ai], F. Suarez [ay], T. Suomijärvi [ae], A.D. Supanitsky [bf], M.S. Sutherland [ch], J. Swain [cg], Z. Szadkowski [bl], J. Takahashi [v], A. Tamashiro [k], A. Tamburro [ao], O. Taşcău [aj], R. Tcaciuc [ap], D. Thomas [cs], R. Ticona [r], J. Tiffenberg [h], C. Timmermans [bi,bg], W. Tkaczyk [bl], C.J. Todero Peixoto [v], B. Tomé [bm], A. Tonachini [aw], I. Torres [bc], D. Torresi [ax], P. Travnicek [ad], A. Tripathi [ck], G. Tristram [af], D. Tscherniakhovski [al], M. Tueros [i], V. Tunnicliffe [bv], R. Ulrich [ak], M. Unger [ak], M. Urban [ag], J.F. Valdés Galicia [bf], I. Valiño [bt], L. Valore [at], A.M. van den Berg [bh], V. van Elewyck [ae], R.A. Vázquez [bt], D. Veberič [bo], A. Veiga [j], A. Velarde [r], T. Venters [cl,af], V. Verzi [au], M. Videla [o], L. Villaseñor [be], S. Vorobiov [bo], L. Voyvodic [cc], H. Wahlberg [j], O. Wainberg [d], P. Walker [bv], D. Warner [ca], A.A. Watson [bw], S. Westerhoff [ct], G. Wieczorek [bl], L. Wiencke [bz], B. Wilczyńska [bk], H. Wilczyński [bk], C. Wileman [bw], M.G. Winnick [p], H. Wu [ag],

B. Wundheiler [b], T. Yamamoto [cl], P. Younk [cs], E. Zas [bt], D. Zavrtanik [bo], M. Zavrtanik [bn], A. Zech [ah], A. Zepeda [bd], M. Ziolkowski [ap]

[a] Centro de Investigaciones en Láseres y Aplicaciones, CITEFA and CONICET, Argentina
[b] Centro Atómico Constituyentes, CNEA, Buenos Aires, Argentina
[c] Centro Atómico Constituyentes, Comisión Nacional de Energía Atómica and CONICET, Argentina
[d] Centro Atómico Constituyentes, Comisión Nacional de Energía Atómica and UTN-FRBA, Argentina
[e] Centro Atómico Bariloche, Comisión Nacional de Energía Atómica, San Carlos de Bariloche, Argentina
[f] Departamento de Física, Centro Atómico Bariloche, Comisión Nacional de Energía Atómica and CONICET, Argentina
[g] Centro Atómico Bariloche, Comision Nacional de Energía Atómica and Instituto Balseiro (CNEA-UNC), San Carlos de Bariloche, Argentina
[h] Departamento de Física, FCEyN, Universidad de Buenos Aires y CONICET, Argentina
[i] Departamento de Física, Universidad Nacional de La Plata and Fundación Universidad Tecnológica Nacional, Argentina
[j] IFLP, Universidad Nacional de La Plata and CONICET, La Plata, Argentina
[k] Instituto de Astronomía y Física del Espacio (CONICET), Buenos Aires, Argentina
[l] Pierre Auger Southern Observatory, Malargüe, Argentina
[m] Pierre Auger Southern Observatory and Comisión Nacional de Energía Atómica, Malargüe, Argentina
[n] Universidad Tecnológica Nacional, FR-Mendoza, Argentina
[o] Universidad Tecnológica Nacional, FR-Mendoza and Fundación Universidad Tecnológica Nacional, Argentina
[p] University of Adelaide, Adelaide, SA, Australia
[q] Universidad Catolica de Bolivia, La Paz, Bolivia
[r] Universidad Mayor de San Andrés, Bolivia
[s] Centro Brasileiro de Pesquisas Fisicas, Rio de Janeiro, RJ, Brazil
[t] Pontifícia Universidade Católica, Rio de Janeiro, RJ, Brazil
[u] Universidade de Sao Paulo, Inst. de Fisica, Sao Paulo, SP, Brazil
[v] Universidade Estadual de Campinas, IFGW, Campinas, SP, Brazil
[w] Univ. Estadual de Feira de Santana, Brazil
[x] Universidade Estadual do Sudoeste da Bahia, Vitoria da Conquista, BA, Brazil
[y] Universidade Federal da Bahia, Salvador, BA, Brazil
[z] Universidade Federal do ABC, Santo André, SP, Brazil
[aa] Univ. Federal do Rio de Janeiro, Instituto de Física, Rio de Janeiro, RJ, Brazil
[ab] Univ. Federal Fluminense, Inst. de Fisica, Niterói, RJ, Brazil
[ac] Charles University, Institute of Particle & Nuclear Physics, Prague, Czech Republic
[ad] Institute of Physics of the Academy of Sciences of the Czech Republic, Prague, Czech Republic
[ae] Institut de Physique Nucléaire, Université Paris-Sud, IN2P3/CNRS, Orsay, France
[af] Laboratoire AstroParticule et Cosmologie, Université Paris 7, IN2P3/CNRS, Paris, France
[ag] Laboratoire de l'Accélérateur Linéaire, Université Paris-Sud, IN2P3/CNRS, Orsay, France
[ah] Laboratoire de Physique Nucléaire et de Hautes Energies, Universités Paris 6 & 7, IN2P3/CNRS, Paris Cedex 05, France
[ai] Laboratoire de Physique Subatomique et de Cosmologie, IN2P3/CNRS, Université Grenoble 1 et INPG, Grenoble, France
[aj] Bergische Universität Wuppertal, Gausstr. 20, 42119 Wuppertal, Germany
[ak] Forschungszentrum Karlsruhe, Institut für Kernphysik, Karlsruhe, Germany
[al] Forschungszentrum Karlsruhe, Institut für Prozessdatenverarbeitung und Elektronik, Germany
[am] Max-Planck-Institut für Radioastronomie, Bonn, Germany
[an] RWTH Aachen University, III. Physikalisches Institut A, Aachen, Germany
[ao] Universität Karlsruhe (TH), Institut für Experimentelle Kernphysik (IEKP), Karlsruhe, Germany
[ap] Universität Siegen, Siegen, Germany
[aq] Università de l'Aquila and Sezione INFN, Aquila, Italy
[ar] Università di Milano and Sezione INFN, Milan, Italy
[as] Università del Salento and Sezione INFN, Lecce, Italy
[at] Università di Napoli "Federico II" and Sezione INFN, Napoli, Italy
[au] Università di Roma II "Tor Vergata" and Sezione INFN, Roma, Italy
[av] Università di Catania and Sezione INFN, Catania, Italy
[aw] Università di Torino and Sezione INFN, Torino, Italy
[ax] Istituto di Astrofisica Spaziale e Fisica Cosmica di Palermo (INAF), Palermo, Italy
[ay] Istituto di Fisica dello Spazio Interplanetario (INAF), Università di Torino and Sezione INFN, Torino, Italy
[az] INFN, Laboratori Nazionali del Gran Sasso, Assergi (L'Aquila), Italy
[ba] Osservatorio Astrofisico di Arcetri, Florence, Italy
[bb] Sezione INFN di Napoli, Napoli, Italy
[bc] Benemérita Universidad Autónoma de Puebla, Puebla, Mexico
[bd] Centro de Investigación y de Estudios Avanzados del IPN (CINVESTAV), México, D.F., Mexico
[be] Universidad Michoacana de San Nicolas de Hidalgo, Morelia, Michoacan, Mexico
[bf] Universidad Nacional Autonoma de Mexico, Mexico, D.F., Mexico
[bg] IMAPP, Radboud University, Nijmegen, Netherlands
[bh] Kernfysisch Versneller Instituut, University of Groningen, Groningen, Netherlands
[bi] NIKHEF, Amsterdam, Netherlands
[bj] ASTRON, Dwingeloo, Netherlands
[bk] Institute of Nuclear Physics PAN, Krakow, Poland

[bl] University of Łódź, Łódz, Poland
[bm] LIP and Instituto Superior Técnico, Lisboa, Portugal
[bn] J. Stefan Institute, Ljubljana, Slovenia
[bo] Laboratory for Astroparticle Physics, University of Nova Gorica, Slovenia
[bp] Instituto de Física Corpuscular, CSIC-Universitat de València, Valencia, Spain
[bq] Universidad Complutense de Madrid, Madrid, Spain
[br] Universidad de Alcalá, Alcalá de Henares (Madrid), Spain
[bs] Universidad de Granada & C.A.F.P.E., Granada, Spain
[bt] Universidad de Santiago de Compostela, Spain
[bu] Rudolf Peierls Centre for Theoretical Physics, University of Oxford, Oxford, United Kingdom
[bv] Institute of Integrated Information Systems, University of Leeds, United Kingdom
[bw] School of Physics and Astronomy, University of Leeds, United Kingdom
[bx] Argonne National Laboratory, Argonne, IL, USA
[by] Case Western Reserve University, Cleveland, OH, USA
[bz] Colorado School of Mines, Golden, CO, USA
[ca] Colorado State University, Fort Collins, CO, USA
[cb] Colorado State University, Pueblo, CO, USA
[cc] Fermilab, Batavia, IL, USA
[cd] Louisiana State University, Baton Rouge, LA, USA
[ce] Michigan Technological University, Houghton, MI, USA
[cf] New York University, New York, NY, USA
[cg] Northeastern University, Boston, MA, USA
[ch] Ohio State University, Columbus, OH, USA
[ci] Pennsylvania State University, University Park, PA, USA
[cj] Southern University, Baton Rouge, LA, USA
[ck] University of California, Los Angeles, CA, USA
[cl] University of Chicago, Enrico Fermi Institute, Chicago, IL, USA
[cm] University of Colorado, Boulder, CO, USA
[cn] University of Hawaii, Honolulu, HI, USA
[co] University of Minnesota, Minneapolis, MN, USA
[cp] University of Nebraska, Lincoln, NE, USA
[cq] University of New Mexico, Albuquerque, NM, USA
[cr] University of Pennsylvania, Philadelphia, PA, USA
[cs] University of Utah, Salt Lake City, UT, USA
[ct] University of Wisconsin, Madison, WI, USA
[cu] University of Wisconsin, Milwaukee, WI, USA
[cv] Institute for Nuclear Science and Technology, Hanoi, Viet Nam

Received 7 December 2007; received in revised form 16 January 2008; accepted 29 January 2008
Available online 10 February 2008

Abstract

A method is developed to search for air showers initiated by photons using data recorded by the surface detector of the Auger Observatory. The approach is based on observables sensitive to the longitudinal shower development, the signal risetime and the curvature of the shower front. Applying this method to the data, upper limits on the flux of photons of 3.8×10^{-3}, 2.5×10^{-3}, and 2.2×10^{-3} km^{-2} sr^{-1} yr^{-1} above 10^{19} eV, 2×10^{19} eV, and 4×10^{19} eV are derived, with corresponding limits on the fraction of photons being 2.0%, 5.1%, and 31% (all limits at 95% c.l.). These photon limits disfavor certain exotic models of sources of cosmic rays. The results also show that the approach adopted by the Auger Observatory to calibrate the shower energy is not strongly biased by a contamination from photons.

1. Introduction

The search for photons in the ultra-high energy (UHE) cosmic-ray flux has been stimulated by the observation of cosmic rays with energies exceeding $E_{\mathrm{GZK}} \sim 6 \times 10^{19}$ eV [1–6]. If these particles are due to cosmologically distant sources, the flux spectrum is expected to steepen above this energy. Intriguingly, a flux spectrum with no apparent steepening above E_{GZK} has been reported by the AGASA Collaboration [7]. To account for this observation and to circumvent the theoretical challenge of explaining particle acceleration to such energies, models involving new physics have been proposed in which the cosmic rays are created at the observed energies at relatively close distances from the Earth. These "top-down" models [8,9] may involve super heavy dark matter (SHDM) [10–12], topological defects [13], or neutrino interactions with the relic neutrino background (Z-bursts) [14]. A common feature of these models

is the prediction of a substantial photon flux at highest energies.

The Auger Collaboration has recently reported a measurement of the cosmic-ray spectrum from the Auger South site showing a flux suppression above E_{GZK} [15]. The Auger method is based on a large surface array to collect the required statistics and a fluorescence detector to calibrate the energy scale. Using this "hybrid" approach, the energy reconstruction is largely independent of hadronic interaction parameters and, in case of nuclear primaries, of the primary mass composition. However, as explained later, the energy assignment from surface arrays can be substantially altered in the case of primary photons. This would affect the reconstructed primary spectrum if a non-negligible number of the highest-energy events, where data from the fluorescence telescopes are sparse due to their ~10% duty cylce, was actually due to photons (see also [16]). It is worthwhile to note that the acceptance of fluorescence detectors (as also applied in the HiRes experiment [5]) can be altered in the case of photon primaries [17–19].

UHE photons can also act as tracers of the GZK (Greisen–Zatsepin–Kuzmin) process [20] of resonant photopion production of nucleons off the cosmic microwave background. The corresponding photon fluxes are sensitive to source features (type of primary, injection spectrum, distance to sources ...) and to propagation parameters (extragalactic radio backgrounds and magnetic fields) [9,21–24].

Thus, the search for primary photons remains an important subject for various reasons [25], particularly

- to set significant limits to the possible contribution of top-down mechanisms to the primary cosmic-ray flux;
- to search for GZK photons, to prove the GZK effect and constrain source and propagation models;
- to establish the maximum photon fraction in the primary flux, for which the energy estimate in the surface array detector would be altered;
- to obtain input to fundamental physics, for instance, to probe quantum gravity effects in the electromagnetic sector [26].

Showers initiated by UHE photons develop differently from showers induced by nuclear primaries. Particularly, observables related to the development stage or "age" of a shower (such as the depth of shower maximum X_{max}) and to the content of shower muons provide good sensitivity to identify primary photons. Photon showers are expected to develop deeper in the atmosphere (larger X_{max}). This is connected to the smaller multiplicity in electromagnetic interactions compared to hadronic ones, such that a larger number of interactions is required to degrade the energy to the critical energy where the cascading process stops. Additionally, the LPM effect [27] results in a suppression of the pair production and bremsstrahlung cross-sections. Photon showers also contain fewer secondary muons, since photoproduction and direct muon pair production are expected to play only a sub-dominant role.

Searches for photons were previously conducted based on surface arrays [28–32], and limits to the fraction of photons were reported (see [25] for a review). The derivation of limits to the photon *fraction* using surface array data alone is an experimental and conceptual challenge (see also Section 2.3). Firstly, for conclusions on the fraction, the energy scales for photon *and* nuclear primaries are needed. These energy scales may differ from each other for surface arrays, and the difference between the scales may depend in a non-trivial way on primary parameters such as the shower zenith angle. Secondly, the energy reconstruction of nuclear primaries suffers from substantial uncertainties due to our limited knowledge of high-energy hadron dynamics.

Both issues can be resolved using the fluorescence technique, which is near-calorimetric and largely independent of simulating hadron interactions. A corresponding approach has been developed and applied recently to obtain a first bound on the fraction of photons from data taken at the Auger Observatory [19].

In this work, using the larger number of events recorded by the surface array, we derive for the first time a direct limit to the *flux* of photons by searching for photon candidates and relating their number to the well-known exposure of the surface array. This avoids the need of simulating events initiated by nuclear primaries; only the photon energy scale is needed which can be simulated with much higher confidence. Two observables of the surface detectors are chosen which have significantly different behavior for nuclear primaries when compared to photons: the risetime of the recorded shower signal and the radius of curvature of the shower front.

We also derive a limit to the fraction of photons. While the challenge of using two energy scales remains for this part of the analysis, hadron simulations can still be avoided by using the hybrid calibration [15] to reconstruct the energies of the observed events.

The plan of the paper is as follows. In Section 2, the observables used in the analysis and their relationship with the composition of cosmic rays are explained. In Section 3, the simulation of UHE photons is considered. The method developed to distinguish events which are photon candidates using observables of the surface detector is detailed in Section 4. In Section 5, the results are presented. The conclusions are given in Section 6.

2. Observables

The analysis in this paper is based on data taken during 21,400 h of operation of the surface detector recorded in the period 1 January 2004 to 31 December 2006. The surface detector, when completed, will have 1600 water Cherenkov detectors spaced 1.5 km apart and covering ~3000 km^2 [33,34]. Each water Cherenkov detector, or station, is a cylinder 1.2 m in height and 3.6 m in diameter. Each detector is lined with a reflective container that holds 12 tonnes of purified water and is fitted with three 9-in. photomultiplier tubes (PMTs) looking down into the water.

When a relativistic particle passes through a station, Cherenkov radiation is emitted. The radiated photons then propagate through the water, being reflected at the station walls, and are either eventually absorbed or detected by a PMT. The signals from the PMTs are digitised by a flash analog to digital converter (FADC) which samples the signal every 25 ns. These digitised signals are then transmitted to a central data acquisition system where event triggers are built. Each event, then, has a detailed time profile $s_i(r_i, t)$ of the energy deposited in each station i at distance r_i in the shower plane. The function $s(r, t)$ depends in a complex way both on the parameters of the primary particle (energy, type, direction) and on the detector response to different secondary particles (particularly the electromagnetic and muonic shower components).

In this work, we extract two relatively simple but robust observables from these data, noting that the wealth of information contained in the time profiles can further be exploited in future work. The observables, the radius of curvature of the shower front and the risetime at 1000 m core distance, were found to provide good discrimination between photon and nuclear primaries (see e.g. also Ref. [35]). In addition to the quantitative studies of these observables by means of the simulation-reconstruction chain, we will also sketch (in a simplified way) why these observables are indeed expected to differ between nuclear and photon primaries.

2.1. Radius of curvature

Due to geometrical reasons, the arrival of the first particles at lateral distance r from the axis is expected to be delayed with respect to an (imaginary) planar shower front (see also Fig. 1, left plot). For a particle that is due to an earlier interaction at height H along the shower axis and observed at r, the delay from the longer path length can be approximated as

$$t = \frac{1}{c}\left(\sqrt{H^2 + r^2} - H\right) \propto \frac{r^2}{H} (r \ll H). \tag{1}$$

The delay increases (for $r \ll H$ about quadratically) with r. Importantly, the delay decreases with increasing height H. Air showers with the first ground particles coming from relatively large heights will have smaller delays t at fixed distance r compared to showers where the registered particles originated from smaller heights. Compared to primary photons, showers from nuclear primaries develop higher in the atmosphere (smaller $X_{\max}$). Additionally, shower muons (much more abundant in showers from nuclear primaries) can reach the ground from still higher altitudes further reducing the time delay. Thus, for nuclear primaries smaller delays are expected compared to photon primaries.

We make use of this relation by fitting a shower front (abstract surface with convex curvature defined by the fastest shower particles) to the measured trigger times $t_i(r_i)$ of the first particles registered at distances r_i. In the present study, the shape of the shower front is approximated using a spherical model (in accord with Eq. (1)), and the radius of curvature R of the shower front is obtained by minimizing χ^2 in the function

$$\chi^2 = \sum_i \frac{[c(t_i - t_0) - |\, R\vec{a} - \vec{x}_i \,|\,]^2}{c^2\sigma_t^2} \tag{2}$$

where t_i is the trigger time for station i as defined in [36], t_0 is the time of the shower in the center of curvature, $\vec{a}$ is the unit vector along the shower axis, $\vec{x}_i$ is the location of the station on the ground relative to the shower core, and σ_t is the uncertainty in the shower arrival time [37]. In the determination of t_i, a software filter is applied to reduce contributions from spurious signals not related to the actual shower.

2.2. Risetime

Also the *spread* in time of the signal $s_i(r_i, t)$ registered at distance r_i, which corresponds to the thickness of the local shower disk, can be extracted. Using Eq. (1), the difference of arrival times of particles originating from a height interval $[H_1, H_1 - \Delta H]$ follows as

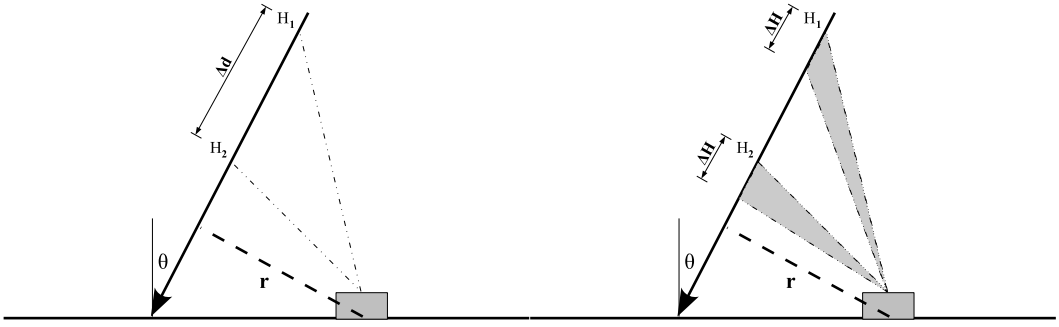

Fig. 1. Illustration of geometrical effects on radius of curvature and risetime of the shower front. (Left) With respect to an imaginary planar shower front, particles arrive more delayed at distance r when originating from a smaller height $H_2 < H_1$. Correspondingly, the radius of curvature of the actual shower front is smaller in case of the deep developing photon primaries. (Right) The spread of arrival times of particles produced over a pathlength ΔH and arriving at distance r increases for a smaller production height $H_2 < H_1$. Correspondingly, the risetime of the shower is increased in case of the deep developing photon primaries.

$$\Delta t(H_1,\Delta H) \propto r^2\left(\frac{1}{H_1-\Delta H}-\frac{1}{H_1}\right)=\frac{r^2\Delta H}{H_1(H_1-\Delta H)} < \Delta t(H_2,\Delta H) \quad \text{for } H_2<H_1. \tag{3}$$

The spread of arrival times of these particles at fixed core distance increases for smaller production heights (see also Fig. 1, right plot). Accordingly, a larger spread is expected in case of the deep developing photon primaries (larger $X_{\max}$). We note that in general, the situation is more complex. The time spread may depend on details of the previous shower development, particularly also on the competition between the signals from the electromagnetic and muonic shower components which will be commented on below. Still, geometrical effects are essential in the relation between time spread and primary composition.

In this study, we use the risetime $t_{1/2}(1000)$ of the shower signal reconstructed for 1000 m distance and located along the line given by the projection of the shower axis onto the ground. First, the risetime $t_{1/2}^{\text{meas}}(r_i)$ of a single station is defined as the time it takes to increase from 10% to 50% of the total signal deposited in that station. According to Eq. (3), for non-vertical showers a (moderate) dependence of $t_{1/2}^{\text{meas}}(r_i)$ on the internal azimuth angle of the stations within the shower plane is expected. This is because the height H measured along the shower axis is larger for those stations on the exterior side of the shower compared to those on the interior side of the shower. To account for this, the observed $t_{1/2}^{\text{meas}}(r_i)$ are corrected depending on the internal azimuth angle ζ of that station:

$$t_{1/2}^{\text{cor}}(r_i)=t_{1/2}^{\text{meas}}(r_i)-g\cdot\cos\zeta \tag{4}$$

$$g=-66.61+95.13\cdot\sec\theta-30.73\cdot\sec^2\theta+[0.001993\cdot\sec\theta-0.001259\cdot\sec^2\theta+0.0002546\cdot\sec^3\theta-0.0009721]\cdot r_i^2$$

where the parameter g depends on distance r and primary zenith angle θ and is parameterised from the data, and ζ is the clockwise angle between the projection of the shower axis on the ground and the line connecting the shower impact point and the station.

It is also expected from Eq. (3) that the values $t_{1/2}^{\text{cor}}(r_i)$ depend on the distance r_i of the stations. We obtain the final risetime $t_{1/2}(1000)$ of the shower by performing a fit to $t_{1/2}^{\text{cor}}(r_i)$ using the function

$$t_{1/2}(r)=(40+ar+br^2)\text{ns}. \tag{5}$$

The parameters a and b are determined for each event by fitting the station data (typical values are 50 ns km^{-1} and 100 ns km^{-2} respectively). The function is anchored at 40 ns at $r=0$ as that is the mean single particle response in the water Cherenkov detectors.

While geometrical effects connected to the different shower developments from nuclear and photon primaries are a main reason for the risetime difference (larger $t_{1/2}(1000)$ in photon showers), again this sensitivity to composition is further strengthened by shower muons which are more abundant in the case of nuclear primaries and can dominate the registered signal at larger zenith angles. As muons tend to arrive within a shorter time window compared to the electromagnetic component which suffers from multiple scattering, this further reduces the risetime $t_{1/2}(1000)$ for nuclear primaries.

2.3. Energy

As an energy estimator, the time-integrated energy deposit $S(1000)$ at 1000 m core distance is used [38]. However, for the same initial energy and direction the average $S(1000)$ from primary photons can be a factor $\geqslant 2$ below that from nuclear primaries [39,40]. Reasons are the (typically factor $\sim$4) smaller number of muons and, due to the later development, the steeper ground lateral distribution in primary photon showers. For a limit to the fraction of primary photons, the energy scales (transformation from $S(1000)$ to primary energy) for both photon and nuclear primaries are required, while the determination of a limit to the flux can rely on the photon energy scale alone.

The energy scale for nuclear primaries is based on the fluorescence technique by using events that are detected with both the surface detector and the fluorescence telescopes [41]. The energy scale for photon primaries (which induce almost purely electromagnetic cascades) is taken from simulations. Thus, both approaches are largely independent from assumptions about hadron interactions at high energy.

Using a direct relationship between $S(1000)$ and primary energy for the photon energy scale results in a (relatively poor) resolution of about 40%. To improve this, a unique energy conversion for photons is applied that is described in detail in Ref. [40]. It is based on the universality of shower development [42], i.e. the electromagnetic part of the shower is expected to develop in a well-predictable manner for depths exceeding $X_{\max}$. In brief, for given values of $S(1000)$ and $X_{\max}$, the primary energy is estimated by

$$\frac{S(1000)}{E_\gamma}=1.4\left(1+\frac{\Delta X-100}{1000}\right)\left[1+\left(\frac{\Delta X-100}{340}\right)^2\right]^{-1} \quad \text{with } \Delta X=X_{\text{ground}}-X_{\max} \tag{6}$$

where $S(1000)$ is measured in units of vertical equivalent muons (VEM) [36], the photon energy E_γ is in EeV, and ΔX is in g cm^{-2}. Since $X_{\max}$ is not directly measured by the surface detector alone, an iterative approach using Eq. (6) is taken to estimate the energy. After an initial guess of the photon energy using $S(1000)$ alone, the typical $X_{\max}$ of the photon showers at this energy is taken from simulations. With this estimate of $X_{\max}$, a new estimate of the photon energy is obtained using Eq. (6), and the procedure is repeated. The energy estimate is found stable after few iterations and an energy resolution of $\sim$25% is achieved [40]. We use this improved estimation of the photon

energy, but note that the main conclusions remain valid also when using a direct energy estimation.

3. Monte Carlo simulations

The QED processes of LPM effect [27] and geomagnetic cascading ([43,35] and references therein) need to be considered for photon showers at highest energy. As mentioned before, the LPM effect leads to a suppression of the pair production and bremsstrahlung cross-sections and, thus, additionally increases the separation of photon and nuclear primaries in terms of $X_{\max}$ (for a review of the LPM effect and experimental observations of the LPM suppression, see [44]).[1] In case of geomagnetic cascading of UHE photons, the initial conversion of the UHE photon into an electron-positron pair can induce a "preshower" (mostly synchrotron photons plus electron–positron pair(s)) outside the atmosphere. The subsequent air showers from such "converted" photons develop higher in the atmosphere (smaller $X_{\max}$) than air showers directly initiated by UHE photons do. As geomagnetic cascading becomes important at energies above $\sim$50 EeV at the southern site of the Auger Observatory, this process is of minor relevance for the bulk of data used in this analysis.

The shower simulations were generated with the Aires simulation package (v2.8), which includes the LPM effect and geomagnetic cascading [45]. QGSJET 01 [46] was used as the hadronic interaction model. The simulation of the water Cherenkov detectors uses the GEANT4 [47] simulation package along with specific code that handles PMT response and data acquisition electronics. The result is that the output of a simulated event is in a format that is identical to the data format recorded with the Auger Observatory. The shower reconstruction procedure used is the same for real events as it is for simulated events to avoid systematic differences at the reconstruction stage.

4. Method

In brief, the limit to the photon flux is obtained as follows. Selection cuts are applied to the data (and simulations) to ensure events of good reconstruction quality and a high acceptance of the detector to photons. Based on $S(1000)$, showers above a minimum primary energy are selected. This data set is then searched for photon candidates using $t_{1/2}(1000)$ and R (see Section 2 for definitions). Simulations assuming photons are used to determine the corresponding selection efficiencies. From the number of photon candidates, the efficiencies with respect to photons, and the experimental exposure (obtained from the geometrical acceptance known from detector monitoring), the upper limit to the photon flux is derived.

[1] Even when artificially switching off the LPM effect, photon showers still have a significantly larger $X_{\max}$ than nuclear primaries (differences $> 150\ \mathrm{g\,cm^2}$ above 10^{19} eV) and a smaller number of muons.

The criteria to select events of good quality are:

- the station with the largest signal is surrounded by six active stations;
- $\geqslant 5$ stations used in the fitting of the lateral distribution function [48] out of which $\geqslant 4$ stations have a non-saturated signal of $\geqslant 10$ VEM (vertical equivalent muons) [36];
- reduced $\chi^2 < 10$ (χ^2 from Eq. (2)).

The first cut restricts the analysis to well-contained events, eliminating in particular events near the border of the array. It affects the geometrical acceptance only. The multiplicity criterion in the second cut is important also to ensure a good reconstruction of $t_{1/2}(1000)$ and R. As the multiplicity is related to primary energy, this cut also affects the energy-dependent acceptance of the array to photons. The third cut rejects the extreme tail of the χ^2 distribution when reconstructing R, removing $\sim$4% of data. As noted before, the assumption of a spherical model used in Eq. (2) is a simplification and, thus, not expected to provide a perfect description of the complex features of the shower front. This cut restricts the analysis to events where a single value of R can be reasonably extracted. It has been checked with simulations that no bias to photons is introduced this way.

As can be seen from Fig. 2, the resulting photon efficiency drops to small values below $\sim$10 EeV. At higher energy, near-vertical photons can also fail the station multiplicity cut due to their deep development. Therefore, the analysis is restricted to

- primary energies $\geqslant 10$ EeV;
- primary zenith angles of 30–60°.

Events with zenith angles below 60° are selected here since inclined showers require dedicated algorithms for an optimum reconstruction [50] (this cut might be relaxed in the future).

The search for photon candidates makes use of $t_{1/2}(1000)$ and R and consists of the following steps. Firstly, the deviation Δ_x of the observable x (with $x = t_{1/2}$ or R referring to risetime or radius of curvature, respectively) from the mean value $\bar{x}_\gamma$ predicted for photons is derived in units of the spread $\sigma_{x,\gamma}$ of the observable x,

$$\Delta_x = \frac{x - \bar{x}_\gamma(S(1000),\theta)}{\sigma_{x,\gamma}(S(1000),\theta)}. \tag{7}$$

where $\bar{x}_\gamma(S(1000),\theta)$ and $\sigma_{x,\gamma}(S(1000),\theta)$ are parameterized from simulations using primary photons. In Fig. 3, examples are shown for these parameterizations of the observables along with distributions of real events.

Secondly, we combine the information contained in the quantities $\Delta_{t_{1/2}}$ and Δ_R by performing a principal component analysis [51], leaving a more sophisticated statistical analysis for the future. To determine the principal component (defined as the axis with the largest variance), 5% of

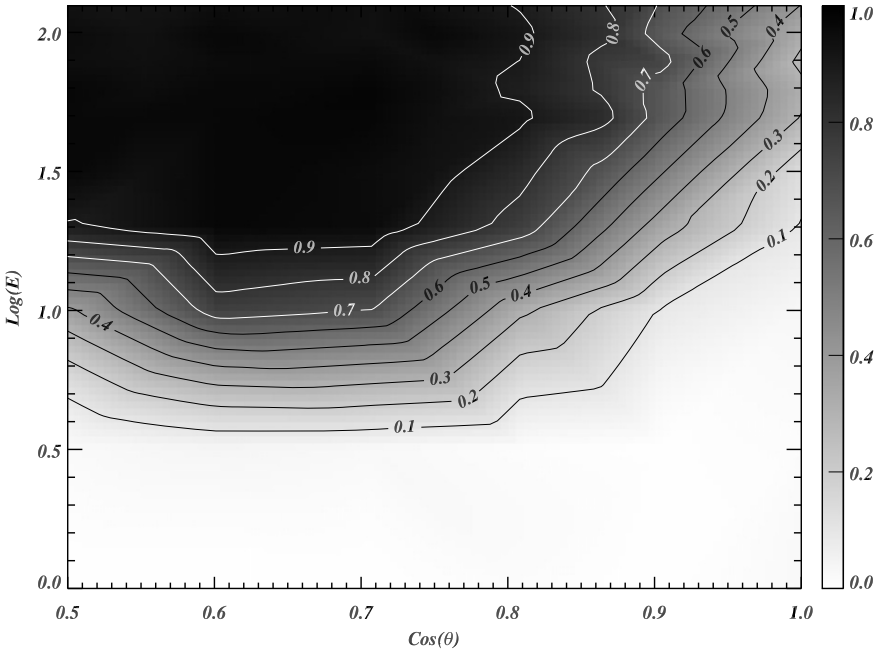

Fig. 2. Photon detection and reconstruction efficiency (right hand scale) as a function of the energy (in EeV) and zenith angle of the primary photon. The analysis is restricted to a minimum energy of 10 EeV and zenith angles greater than 30° and less than 60° ($0.866 > \cos\theta > 0.5$).

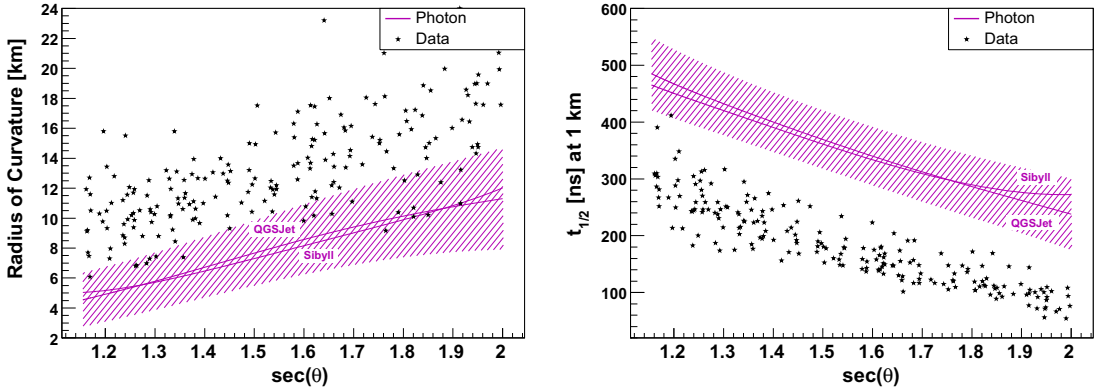

Fig. 3. Parameterization of the mean behavior of R and $t_{1/2}$ for 20 EeV primary photons as a function of the zenith angle using QGSJET 01 [46] or SIBYLL 2.1 [49]. The rms values are indicated for the case of QGSJET 01. An increase (a decrease) of R (of $t_{1/2}$) with zenith angle is qualitatively expected from Eqs. (1) and (3) due to the generally longer path lengths to ground in case of larger inclination. Real events of 19–21 EeV (photon energy scale) are added. The significant deviation of the observed values from those expected for primary photons is visible.

the real events are used together with results from photon simulations, see Fig. 4. For the simulations, a power law spectrum of index −2.0 has been assumed (see below for other indices). The remaining 95% of the data are then projected onto the principal axis along with the simulated photons.

This procedure allows the *a priori* definition of a simple cut in the projected distribution to finally obtain photon candidate events. The cut was chosen at the mean of the distribution for photons, such that the efficiency of this cut is $f = 0.5$ by construction. Any real event falling above this cut will be considered a photon candidate. We note that such photon candidates, if occurring, can not yet be considered as being photons, as they actually might be due to background events from nuclear primaries. A presence of background events would result in weaker upper limits (larger numerical values) in the analysis approach adopted here.

Finally, an upper limit on the number of photons $\mathcal{N}_\gamma^{\mathrm{CL}}$ at confidence level CL is calculated from the number of photon candidate events N_γ above a minimum energy, E_{min}. The upper limit on the flux or fraction of photons above a given energy is based on $\mathcal{N}_\gamma^{\mathrm{CL}}$ along with the integrated efficiency ε of accepting photons, the photon selection cut efficiency ($f = 0.5$), and either the exposure A of the detector for the flux limit:

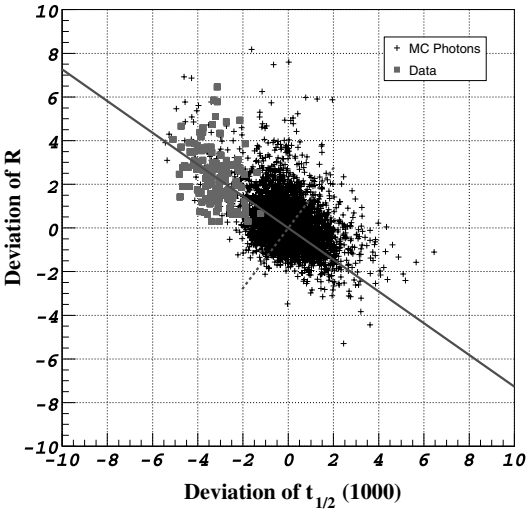

Fig. 4. The deviation from a photon prediction for 5% of the data (closed squares) and simulated photon events (crosses). The solid grey line is the principal component axis identified using the limited set of real showers while the dashed line is the axis perpendicular to the principal component. The minimum energy is 10 EeV ($E_\gamma > 10$ EeV).

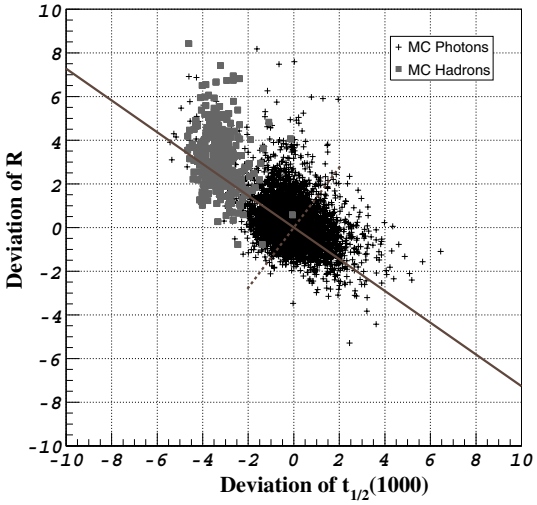

Fig. 5. The black crosses are simulated photon showers while the squares are a mixture of Monte Carlo proton and iron with an energy of 10 EeV. For comparison, the lines shown in Fig. 4 (principal component axes) are added. The distribution of simulated nuclear primaries is similar to the distribution of real data seen in Fig. 4.

$$\Phi_{\rm CL}(E > E_{\rm min}) = \frac{\mathcal{N}_\gamma^{\rm CL}(E_\gamma > E_{\rm min}) \times \frac{1}{f} \times \frac{1}{\varepsilon}}{0.95A}, \tag{8}$$

or the number of non-photon candidate events $N_{\text{non-}\gamma}$ in the data set for the fraction limit:

$$\mathcal{F}_{\rm CL}(E > E_{\rm min}) = \frac{\mathcal{N}_\gamma^{\rm CL}(E_\gamma > E_{\rm min}) \times \frac{1}{f} \times \frac{1}{\varepsilon}}{N_\gamma(E_\gamma > E_{\rm min}) + N_{\text{non-}\gamma}(E_{\text{non-}\gamma} > E_{\rm min})}. \tag{9}$$

In Eq. (8), the factor 0.95 is from the fact that only 95% of the data are used to determine the number of photon candidate events. The energy is labeled as either the energy according to the photon energy reconstruction, E_γ, or (required in Eq. (9)) the energy according to the non-photon energy reconstruction, $E_{\text{non}-\gamma}$.

Experimentally, the limit $\Phi_{\rm CL}$ to the flux is more robust than the limit $\mathcal{F}_{\rm CL}$ to the fraction due to the different denominators of Eqs. (8) and (9). For $\mathcal{F}_{\rm CL}$, two energy scales are required; also, with increasing energy, the statistical uncertainty of the quantity $(N_\gamma + N_{\text{non-}\gamma})$ becomes large. For $\Phi_{\rm CL}$, in contrast, the aperture is known to good ($\sim$3%) accuracy.

Though the present work does not aim at extracting a composition of nuclear primaries, it is interesting to check whether the principal component axis found from real data and the separation along it reflects what would be expected if the bulk of the real data is due to nuclear primaries. In Fig. 5, the same simulated photon events are used as in Fig. 4 but the 5% of real data are replaced with a set of $\sim$750 Monte Carlo proton and iron showers with an energy of 10 EeV. The separation observed in real data is both in the same direction and of a similar magnitude as that expected from simulated nuclear primaries.

5. Results

The data from 2004–2006 are analysed as described in the preceding section. The integrated aperture of the Observatory is 3130 km^2 sr yr for the angular coverage regarded in this analysis. Above 10, 20, and 40 EeV, for the energy scale of photons (in brackets for nuclear primaries), the data set consists of 2761 (570), 1329 (145), and 372 (21) events. The measured values of $t_{1/2}(1000)$ and R are used to determine the projection on the principal axis. A scatter plot of this quantity vs. the primary energy is shown in Fig. 6, while in Fig. 7 the corresponding distribu-

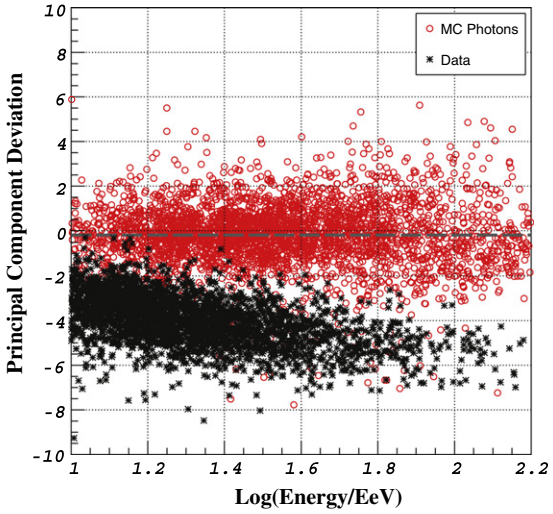

Fig. 6. The deviation of data (black crosses) and photons (open red circles) from the principal component as a function of the primary energy (photon energy scale). Data lying above the dashed line, which indicates the mean of the distribution for photons, are taken as photon candidates. No event meets this requirement.

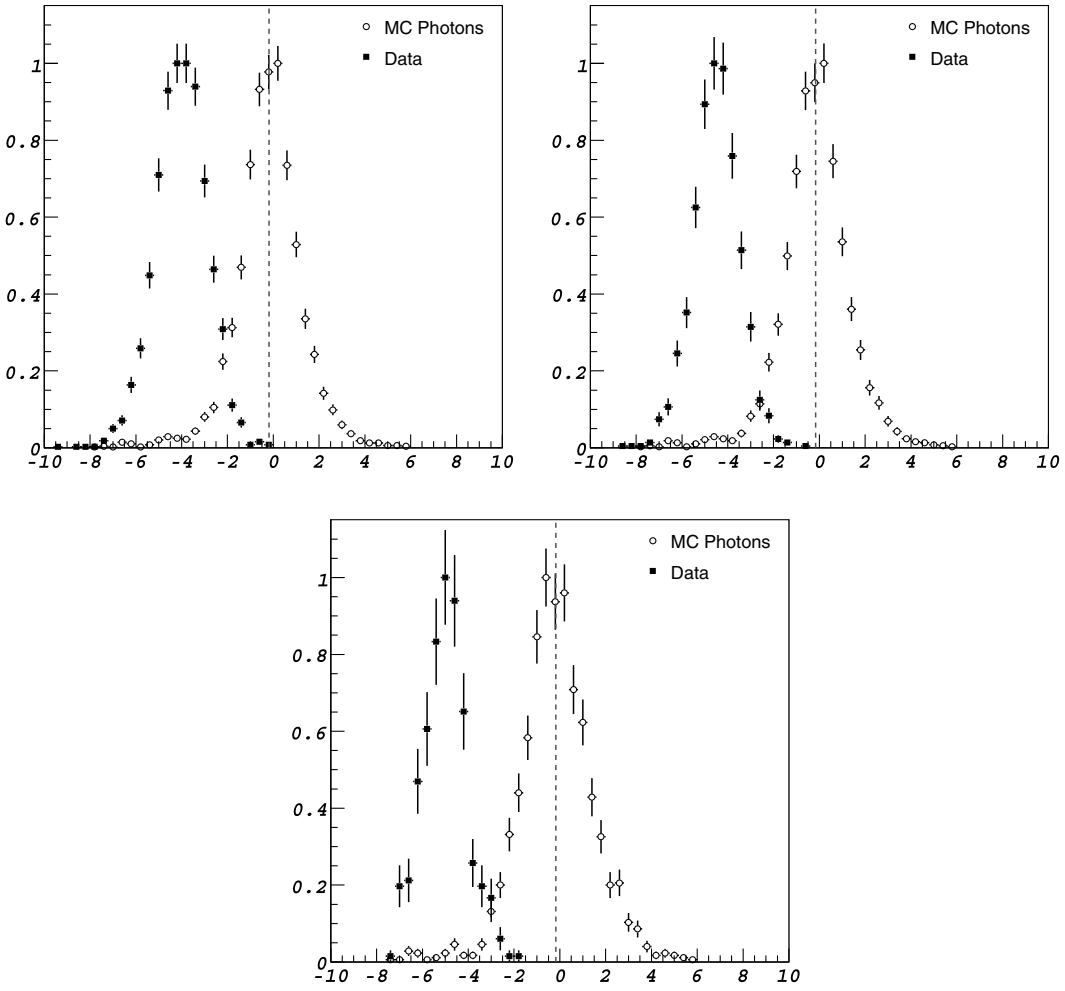

Fig. 7. Distribution of real events (closed squares) along with simulated photon events (open circles) for the projection on the principal component axis. The photon candidate cut is set at the mean of the distribution for photons and is shown as the dotted line. The plots are made requiring a minimum energy (according to the photon energy converter) of 10 EeV (top-left), 20 EeV (top-right), and 40 EeV (bottom). Distributions are normalised to unity at maximum.

tions are plotted for the three threshold energies. No event passes the photon candidate cut. The upper limits on the photon flux above 10, 20, and 40 EeV are then 3.8×10^{-3}, 2.5×10^{-3}, and 2.2×10^{-3} km^{-2} sr^{-1} yr^{-1} (at 95% CL). The limits on the photon fraction are 2.0%, 5.1%, and 31% (at 95% CL) above 10, 20, and 40 EeV. In Table 1, all relevant quantities (number of events, efficiencies, resulting limits) are summarized.

From Fig. 6 it can also be seen that the separation of data and photon primaries increases with energy. In particular at highest energies above E_{GZK} for the photon energy scale, there is no indication for photon-initiated events. Thus, the absence of photons, within the improved limits placed in this work, shows that the method applied by the Auger Observatory to calibrate the shower energy is not strongly biased by a photon "contamination".

Table 1
Results of the analysis searching for photon candidate events

E_{min}	$N(E_\gamma > E_{\mathrm{min}})$	N_γ	$\mathcal{N}_\gamma^{0.95}$	$N_{\text{non-}\gamma}$	ε	$\Phi_{0.95}$	$\mathcal{F}_{0.95}$ (%)
10	2761	0	3.0	570	0.53	3.8×10^{-3}	2.0
20	1329	0	3.0	145	0.81	2.5×10^{-3}	5.1
40	372	0	3.0	21	0.92	2.2×10^{-3}	31

The fraction and flux limits are integral limits above E_{min}(EeV), ε is the efficiency of detection and reconstruction, $\Phi_{0.95}$ is in units of km^{-2} sr^{-1} yr^{-1}, and limits are at 95% confidence level.

We studied potential sources of systematic effects in the analysis. To determine the efficiency to photons and to establish the photon candidate cut, a primary photon spectrum of power law index -2.0 has been used in the simulations, motivated by predictions from top-down models in (e.g. in Ref. [10]). The effect of changing the power law index to -1.7, -2.5, and -3.0 has been investigated. The number of events which are photon candidates is unchanged (along with the number of non-photon candidate events), but the correction for the photon efficiency changes. Specifically, for a steeper input spectrum (increased fraction of lower-energy photons), the efficiency decreases. The summary of the results can be seen in Table 2. For 10 EeV threshold energy, limits change from $(3.8 \rightarrow 5.5) \times 10^{-3}$ km^{-2} sr^{-1} yr^{-1} for the flux and from $(2.0 \rightarrow 2.9)$% for the fraction. The differences get smaller with increased threshold energy.

Table 2
Results when changing the exponent (α) in the power law of the simulated spectrum

E_{min}	10	20	40	10	20	40	10	20	40
α	Efficiency (ε)			Flux ($\times 10^{-3}$)			Fraction (%)		
1.7	0.60	0.83	0.93	3.3	2.4	2.2	1.8	5.0	31
2.0	0.53	0.81	0.92	3.8	2.5	2.2	2.0	5.1	31
2.5	0.43	0.76	0.91	4.7	2.6	2.2	2.5	5.4	31
3.0	0.36	0.71	0.90	5.5	2.8	2.2	2.9	5.9	32

The default value is 2.0. The efficiency of detection and reconstruction is on the left, the resulting limit on the fraction of photons is on the right, and the limit on the integrated flux is listed in the middle in units of km^{-2} sr^{-1} yr^{-1} (95% CL).

The photonuclear cross-section used in the simulation is based on the Particle Data Group (PDG) extrapolation [52]. For an increased cross-section, more energy would be transferred to the hadron (and muon) component which could diminish the separation power between data and primary photons [53]. From unitarity constraints, the cross-section is not expected to exceed the PDG extrapolation by more than ~75% at 10 EeV [54]; at 10^{15} eV, where the difference in cross-section would have a greater impact on the shower development, the maximum difference is ~20%. From simulations with modified cross-sections it was verified that this leads to a negligible variation of the average values of the discriminating variables used in the current analysis.

The simulations have been performed with AIRES using the QGSJET hadronic interaction model. As a cross-check, calculations with CORSIKA [55]/QGSJET and AIRES/SIBYLL were conducted, both of which show reasonable agreement to the AIRES/QGSJET case. As the cascade initiated by primary photons has an almost pure electromagnetic nature, indeed no significant effect is expected when changing to another interaction model. This minor dependence of the results on the details of hadron interactions, which are largely uncertain at high energy, is an important advantage of searches for primary photons.

The new limits are compared to previous results and to theoretical predictions in Fig. 8 for the photon flux and in Fig. 9 for the photon fraction. We placed the first direct limit to the flux of UHE photons (an earlier bound from AGASA, about an order of magnitude weaker than the current bounds, was derived indirectly via a limit to the fraction and the flux spectrum [29]). In terms of the photon fraction, the current bound at 10 EeV approaches the 10^{-2} level while previous bounds were at the 10^{-1} level.

A discovery of a substantial photon flux could have been interpreted as a signature of top-down models. In turn, the experimental limits now put strong constraints on these models. For instance, certain SHDM or TD models discussed in the literature (SHDM and TD from Ref. [21] based on the fragmentation calculations of Ref. [11], SHDM' from Ref. [12][2]) predict fluxes that exceed the limits by a factor ~10. It should be noted that a simple rescaling of the flux predictions from top-down models, which were motivated by and based on the energy spectrum observed by AGASA, would reduce the predicted photon flux by only a factor ~2 which would still overshoot our experimental limit by a factor ~5 at 10^{19} eV. While a minor contribution from top-down models to the observed UHE cosmic-ray flux might still be allowed within the limits derived in this work, current top-down models do not appear to provide an adequate explanation of the origin of the highest-energy cosmic rays (see also Ref. [56] for a comparison of photon flux predictions to the Auger limits for different top-down model parameters).

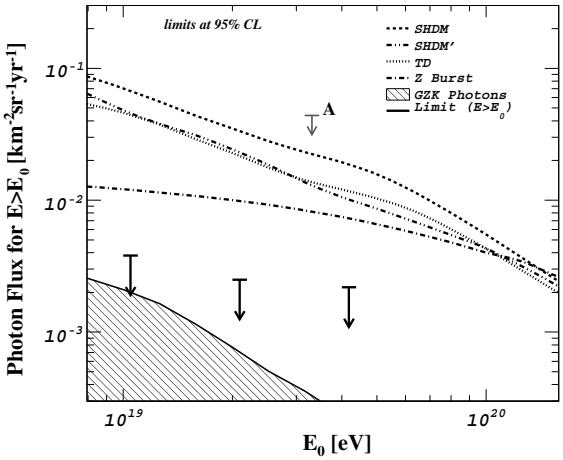

Fig. 8. The upper limits on the integral flux of photons derived in this work (black arrows) along with predictions from top-down models (SHDM, TD and ZB from Ref. [21], SHDM' from Ref. [12]) and with predictions of the GZK photon flux [21]. A flux limit derived indirectly by AGASA ("A") is shown for comparison [29].

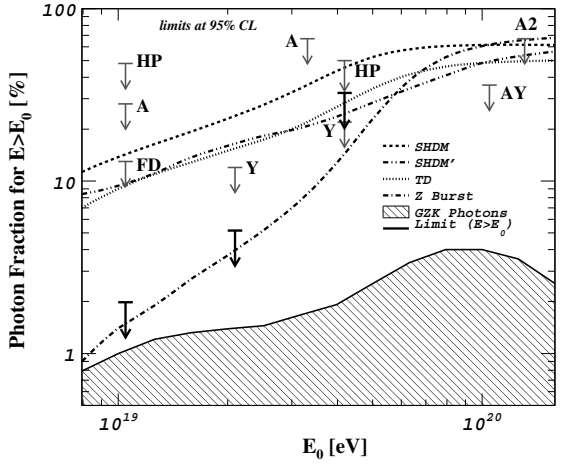

Fig. 9. The upper limits on the fraction of photons in the integral cosmic-ray flux derived in this work (black arrows) along with previous experimental limits (HP: Haverah Park [28]; A1, A2: AGASA [29,30]; AY: AGASA-Yakutsk [31]; Y: Yakutsk [32]; FD: Auger hybrid limit [19]). Also shown are predictions from top-down models (SHDM, TD and ZB from Ref. [21], SHDM' from Ref. [12]) and predictions of the GZK photon fraction [21].

[2] Two others of the eight photon flux spectra calculated in Ref. [12] from crypton decays may still be compatible with our limits within a factor ~2.

In acceleration models, photon fluxes are usually expected to be a factor 2 or more below the current bounds (cf. the GZK photon predictions in the Figs. 8 and 9 from Ref. [21]). Such fluxes can be tested with future data taken at the Auger Observatory (see also Ref. [25]). After 5 years of operation with the complete surface detector, sensitivities at the level of $\sim 4 \times 10^{-4}$ km^{-2} sr^{-1} yr^{-1} for the integrated flux and $\sim$0.7% for the fraction of photons above 20 EeV (95% CL) could be reached.

6. Conclusions

Using data from the surface detector we obtained 95% c.l. upper limits on the photon flux of 3.8×10^{-3}, 2.5×10^{-3}, and 2.2×10^{-3} km^{-2} sr^{-1} yr^{-1} above 10^{19} eV, 2×10^{19} eV, and 4×10^{19} eV. These are the first direct bounds on the *flux* of UHE photons. For the photon fraction, limits of 2.0%, 5.1%, and 31% were placed.

These limit improve significantly upon bounds from previous experiments and put strong constraints on certain models of the origin of cosmic rays. Current top-down models such as the super-heavy dark matter scenario do not appear to provide an adequate explanation of the UHE cosmic rays. In bottom-up models of acceleration of nuclear primaries in astrophysical sources, the expected photon fluxes are typically well below the current bounds. An astrophysical origin of UHE cosmic rays is also suggested by the recent discovery of a correlation of UHE cosmic rays with the directions of nearby AGNs [57]. Concerning the method of energy calibration as applied by the Auger Observatory, the photon bounds derived in this work show that there is no strong bias due to a contamination from UHE photons.

With the data accumulating over the next years, and particularly when complementing the Auger southern site by an extended northern one, the flux levels expected for GZK photons may be in reach.

Acknowledgements

The successful installation and commissioning of the Pierre Auger Observatory would not have been possible without the strong commitment and effort from the technical and administrative staff in Malargüe.

We are very grateful to the following agencies and organizations for financial support: Comisión Nacional de Energía Atómica, Fundación Antorchas, Gobierno De La Provincia de Mendoza, Municipalidad de Malargüe, NDM Holdings and Valle Las Leñas, in gratitude for their continuing cooperation over land access, Argentina; the Australian Research Council; Conselho Nacional de Desenvolvimento Científico e Tecnológico (CNPq), Financiadora de Estudos e Projetos (FINEP), Fundação de Amparo à Pesquisa do Estado de Rio de Janeiro (FAPERJ), Fundação de Amparo à Pesquisa do Estado de São Paulo (FAPESP), Ministério de Ciência e Tecnologia (MCT), Brazil; Ministry of Education, Youth and Sports of the Czech Republic; Centre de Calcul IN2P3/CNRS, Centre National de la Recherche Scientifique (CNRS), Conseil Régional Ile-de-France, Département Physique Nucléaire et Corpusculaire (PNC-IN2P3/CNRS), Département Sciences de l'Univers (SDU-INSU/CNRS), France; Bundesministerium für Bildung und Forschung (BMBF), Deutsche Forschungsgemeinschaft (DFG), Finanzministerium Baden-Württemberg, Helmholtz-Gemeinschaft Deutscher Forschungszentren (HGF), Ministerium für Wissenschaft und Forschung, Nordrhein-Westfalen, Ministerium für Wissenschaft, Forschung und Kunst, Baden-Württemberg, Germany; Istituto Nazionale di Fisica Nucleare (INFN), Ministero dell'Istruzione, dell'Università e della Ricerca (MIUR), Italy; Consejo Nacional de Ciencia y Tecnología (CONACYT), Mexico; Ministerie van Onderwijs, Cultuur en Wetenschap, Nederlandse Organisatie voor Wetenschappelijk Onderzoek (NWO), Stichting voor Fundamenteel Onderzoek der Materie (FOM), Netherlands; Ministry of Science and Higher Education, Grant Nos. 1 P03 D 014 30, N202 090 31/0623, and PAP/218/2006, Poland; Fundação para a Ciência e a Tecnologia, Portugal; Ministry for Higher Education, Science, and Technology, Slovenian Research Agency, Slovenia; Comunidad de Madrid, Consejería de Educación de la Comunidad de Castilla La Mancha, FEDER funds, Ministerio de Educación y Ciencia, Xunta de Galicia, Spain; Science and Technology Facilities Council, United Kingdom; Department of Energy, Contract No. DE-AC02-07CH11359, National Science Foundation, Grant No. 0450696, The Grainger Foundation USA; ALFA-EC/HELEN, European Union 6th Framework Program, Grant No. MEIF-CT-2005-025057, and UNESCO.

References

[1] J. Linsley, Phys. Rev. Lett. 10 (1963) 146.
[2] M.A. Lawrence, R.J.O. Reid, A.A. Watson, J. Phys. G17 (1991) 733.
[3] D.J. Bird et al., Phys. Rev. Lett. 71 (1993) 3401.
[4] N. Hayashida et al., Phys. Rev. Lett. 73 (1994) 3491.
[5] R.U. Abbasi et al., Phys. Lett. B 619 (2005) 271.
[6] Pierre Auger Collaboration, in: Proceedings of the 29th International Cosmic Ray Conference, Pune, vol. 7, 2005, p. 283.
[7] M. Takeda et al., Astropart. Phys. 19 (2003) 447.
[8] P. Bhattacharjee, G. Sigl, Phys. Rep. 327 (2000) 109.
[9] S. Sarkar, Acta Phys. Polon. B35 (2004) 351.
[10] V. Berezinsky, M. Kachelrieß, A. Vilenkin, Phys. Rev. Lett. 79 (1997) 4302;
M. Birkel, S. Sarkar, Astropart. Phys. 9 (1998) 297;
S. Sarkar, R. Toldra, Nucl. Phys. B 621 (2002) 495;
C. Barbot, M. Drees, Astropart. Phys. 20 (2003) 5;
R. Aloisio, V. Berezinsky, M. Kachelriess, Phys. Rev. D 74 (2006) 023516.
[11] R. Aloisio, V. Berezinsky, M. Kachelriess, Phys. Rev. D 69 (2004) 094023.
[12] J. Ellis, V. Mayes, D.V. Nanopoulos, Phys. Rev. D 74 (2006) 115003.
[13] C.T. Hill, Nucl. Phys. B 224 (1983) 469;
M.B. Hindmarsh, T.W.B. Kibble, Rep. Prog. Phys. 58 (1995) 477.
[14] T.J. Weiler, Phys. Rev. Lett. 49 (1982) 234;
T.J. Weiler, Astropart. Phys. 11 (1999) 303;
D. Fargion, B. Mele, A. Salis, Astrophys. J. 517 (1999) 725.

[15] Pierre Auger Collaboration, in: Proceedings of the 30th International Cosmic Ray Conference, Merida, 2007. Available from: astro-ph/0706.2096.
[16] N. Busca, D. Hooper, E.W. Kolb, Phys. Rev. D 73 (2006) 123001.
[17] V. de Souza, G. Medina-Tanco, J.A. Ortiz, Phys. Rev. D 72 (2005) 103009.
[18] A.S. Chou, Phys. Rev. D 74 (2006) 103001.
[19] Pierre Auger Collaboration, Astropart. Phys. 27 (2007) 155;
Pierre Auger Collaboration, in: Proceedings of the 30th International Cosmic Ray Conference, Merida, 2007. Available from: astro-ph/0710.0025.
[20] K. Greisen, Phys. Rev. Lett. 16 (1966) 748;
G.T. Zatsepin, V.A. Kuzmin, JETP Lett. 4 (1966) 78.
[21] G. Gelmini, O.E. Kalashev, D.V. Semikoz. Available from: astro-ph/0506128.
[22] S. Lee, A.V. Olinto, G. Sigl, Astrophys. J. 455 (1995) L21.
[23] G. Sigl, Phys. Rev. D 75 (2007) 103001. Available from: astro-ph/0703403.
[24] G. Gelmini, O. Kalashev, D.V. Semikoz. Available from: astro-ph/0706.2181.
[25] M. Risse, P. Homola, Mod. Phys. Lett. A 22 (2007) 749.
[26] M. Galaverni, G. Sigl, Phys. Rev. Lett. 100 (2008) 021102. Available from: astro-ph/0708.1737.;
R. Aloisio, P. Blasi, P.L. Ghia, A.F. Grillo, Phys. Rev. D 62 (2000) 053010. Available from: arXiv:astro-ph/0001258.
[27] L.D. Landau, I.Ya. Pomeranchuk, Dokl. Akad. Nauk SSSR 92 (1953) 535, also p. 735;
A.B. Migdal, Phys. Rev. 103 (1956) 1811.
[28] M. Ave et al., Phys. Rev. Lett. 85 (2000) 2244;
M. Ave et al., Phys. Rev. D 65 (2002) 063007.
[29] K. Shinozaki et al., Astrophys. J. 571 (2002) L117.
[30] M. Risse et al., Phys. Rev. Lett. 95 (2005) 171102.
[31] G.I. Rubtsov et al., Phys. Rev. D 73 (2006) 063009.
[32] A.V. Glushkov et al., JETP Lett. 85 (2007) 163.
[33] Pierre Auger Collaboration, Nucl. Instrum. Methods A 523 (2004) 50.
[34] Pierre Auger Collaboration, in: Proceedings 30th International Cosmic Ray Conference, Merida, 2007. Available from: astro-ph/0709.1823.
[35] X. Bertou, P. Billoir, S. Dagoret-Campagne, Astropart. Phys. 14 (2000) 121.
[36] X. Bertou et al., P. Auger Collaboration, Nucl. Instrum. Methods A 568 (2006) 839.
[37] Pierre Auger Collaboration, in: Proceedings 29th International Cosmic Ray Conference, Pune, vol. 7, 2005, p. 17.
[38] D. Newton, J. Knapp, A.A. Watson, Astropart. Phys. 26 (2007) 414.
[39] Pierre Auger Collaboration, in: Proceedings 29th International Cosmic Ray Conference, Pune, vol. 7, 2005, p. 387. Available from: astro-ph/0507150.
[40] P. Billoir, C. Roucelle, J.C. Hamilton. Available from: astro-ph/0701583.
[41] Pierre Auger Collaboration, in: Proceedings 30th International Cosmic Ray Conference, Merida. Available from: astro-ph/0706.1105.
[42] A.S. Chou et al., in: Proceedings 29th International Cosmic Ray Conference, Pune, vol. 7, 2005, p. 319.
[43] T. Erber, Rev. Mod. Phys. 38 (1966) 626;
B. McBreen, C.J. Lambert, Phys. Rev. D 24 (1981) 2536;
T. Stanev, H.P. Vankov, Phys. Rev. D 55 (1997) 1365;
P. Homola et al., Comput. Phys. Commun. 173 (2005) 71;
P. Homola et al., Astropart. Phys. 27 (2007) 174.
[44] S. Klein, Rev. Mod. Phys. 71 (1999) 1501;
S. Klein, Rad. Phys. Chem. 75 (2006) 696.
[45] S.J. Sciutto, AIRES: a system for air shower simulations (version 2.2.0). Available from: astro-ph/9911331; available at http://www.fisica.unlp.edu.ar/auger/aires.
[46] N.N. Kalmykov, S.S. Ostapchenko, A.I. Pavlov, Nucl. Phys. B (Proceedings Suppl.) 52B (1997) 17.
[47] S. Agostinelli et al., Nucl. Instrum. Methods A 506 (2003) 250;
J. Allison et al., IEEE Transactions on Nuclear Science 53 (2006) 270, See also http://geant4.cern.ch/.
[48] Pierre Auger Collaboration, in: Proceedings of the 29th International Cosmic Ray Conference, Pune, vol. 7, 2005, p. 291.
[49] R. Engel, T.K. Gaisser, P. Lipari, T. Stanev, Proceedings 26th International Cosmic Ray Conference, Salt Lake City 1 (1999) 415.
[50] Pierre Auger Collaboration, in: Proceedings 30th International Cosmic Ray Conference, Merida, 2007. Available from: astro-ph/0706.2096.
[51] E. Oja, Int. J. Neural Syst. 1 (1989) 61.
[52] S. Eidelmann et al., Particle Data Group, Phys. Lett. B592 (2004) 1.
[53] M. Risse et al., Czech. J. Phys. 56 (2006) A327.
[54] T.C. Rogers, M.I. Strikman, J. Phys. G: Nucl. Part. Phys. 32 (2006) 2041.
[55] D. Heck et al., Reports FZKA 6019 & 6097, Forschungszentrum Karls-ruhe (1998).
[56] Pierre Auger Collaboration, in: Proceedings 30th International Cosmic Ray Conference, Merida, 2007. Available from: astro-ph/0706.2960.
[57] Pierre Auger Collaboration, Science 318 (2007) 939.